
Multiple Domain Causal Networks

Tianhui Zhou¹, William E. Carson IV², Michael Hunter Klein³, David Carlson^{1,3,4}

¹Department of Biostatistics and Bioinformatics

²Department of Biomedical Engineering

³Department of Electrical and Computer Engineering

⁴Department of Civil and Environmental Engineering

Duke University

Durham, NC 27708

{tianhui.zhou, wecl4, michael.klein413, david.carlson}@duke.edu

Abstract

Observational studies are regarded as economic alternatives to randomized trials, often used in their stead to investigate and determine treatment efficacy. Due to lack of sample size, observational studies commonly combine data from multiple sources or different sites/centers. Despite the benefits of an increased sample size, a naïve combination of multicenter data may result in incongruities stemming from center-specific protocols for generating cohorts or reactions towards treatments distinct to a given center, among other things. These issues arise in a variety of other contexts, including capturing a treatment effect related to an individual’s unique biological characteristics. Existing methods for estimating heterogeneous treatment effects have not adequately addressed the multicenter context, but rather treat it simply as a means to obtain sufficient sample size. Additionally, previous approaches to estimating treatment effects do not straightforwardly generalize to the multicenter design, especially when required to provide treatment insights for patients from a new, unobserved center. To address these shortcomings, we propose Multiple Domain Causal Networks (MDCN), an approach that simultaneously strengthens the information sharing between similar centers while addressing the selection bias in treatment assignment through learning of a new feature embedding. In empirical evaluations, MDCN is consistently more accurate when estimating the heterogeneous treatment effect in new centers compared to benchmarks that adjust solely based on treatment imbalance or general center differences. Finally, we justify our approach by providing theoretical analyses that demonstrate that MDCN improves on the generalization bound of the new, unobserved target center.

1 Introduction

Recent advancements in deep learning have facilitated characterization and modeling of complex relationships [36, 40]. Accordingly, deep learning has since been applied to problems of personalized medicine, with the goal to accurately quantify each individual’s heterogeneous response to a given treatment [24]. Due to the high cost of conducting experiments, researchers often turn to observational data to find clues through building predictive models or making quantitative assessments [10]. To enlarge the overall sample size, data collected from multiple different centers (clusters) are combined. This practice is commonly referred to as a “multicenter observational study” [14]. Naïvely combining data from multiple sources or ignoring the underlying cluster structure can be problematic. For example, individuals from different centers could have distinctive feature distributions with minimum overlap. Moreover, the mechanisms underlying treatment selection bias may differ from center to center. The combination of these issues present a challenge to researchers attempting to quantitatively model the effects of treatment assignment of patients from a new center. Limited work has been

conducted for the causal estimation in a multicenter setting [46], as the vast majority of existing approaches address only part of the problem. To bridge this gap, our goal is to design a framework that jointly addresses the structural considerations of multicenter data *and* robust estimation of heterogeneous treatment effects for individuals from new centers.

Different centers or different treatment groups within a same center could mathematically be described as feature spaces $X \in \mathcal{X}$ of different distributions. This aligns with the definition of “domain” in the domain adaptation literature where the similarity among different domains are leveraged to improve a model’s generalization [6]. Inspired by the idea, we propose Multiple Domain Causal Networks (MDCN): a novel approach that takes into account both *selection bias in treatment assignment* and *discrepancies inherent to data collected at different centers*. Succinctly, we employ domain adaptation to simultaneously increase the overlap between treatment groups and match centers with more similarities to gain robustness in inference. Moving forward, we will use “domain” to refer to a center or cluster from which data was collected. Not only can the proposed approach be applied to data collected from multiple medical centers, but it can also be used in broader contexts (e.g., considering individuals as separate domains). For instance, we motivate our method using neural data collected from mice, where behavioral assays can be framed as treatment regimes and we expect heterogeneous treatment effects between individual mice. This approach is highly relevant to observational studies that evaluate the impact of pharmaceuticals [12] or other interventions based on brain measurements (e.g. neurostimulation [9]). Our main contributions include the following:

1. We formulate the heterogeneous treatment effect estimation problem under the context of multicenter observational studies.
2. We propose a new representation learning approach that accounts for both domain-level discrepancies and selection biases in treatment assignment.
3. We provide supporting theoretical proof demonstrating that the error on the new, unobserved target center is bounded with the proposed method.

2 Related Work

To date, few works address out-of-domain treatment effect estimation, especially on multicenter data. One example is generalized mixed effect models that handle cluster-structured data derived from multiple domains [13, 34]; however, this approach is an additive linear model that requires specific likelihood functions for its mean model and variance model, which restricts customization and is less capable of handling heterogeneous relationships. Instead, we will build on recent advances in using machine learning for causal estimation and in domain adaption, briefly described below.

There are many recent advances in machine learning for causal inference. A variety of methods have been used, including methods that match individuals [3, 8, 38] or parts of the covariate space (e.g. tree-based methods [2, 22]). A critical issue in causal inference is mismatch of the covariate space, motivating weighting methods [1, 28]). Rather than weighting all samples, one could disentangle the confounding effect from the feature space [26, 53], find a more balanced embedding between treatment groups [41], or embed the treatment assignment mechanism in a new latent representation [20, 43]. Despite demonstrable improvement in model generalization for causal inference, these models do not account for multiple domain setups and their extensions to out-of-domain prediction are not straightforward.

Domain adaptation methods provide elegant solutions to account for the inherent distribution shift across different domains [4, 48, 49, 54]. Many domain adaptation methods aim to find a latent variable representation where the distributions of multiple domains are matched [55]. Matched latent domains can be learned by penalizing with statistical measures such as the Maximum Mean Discrepancy [7] or Wasserstein Distance [42], or by matching second order statistics [47]. Another family of techniques make use of adversarial methods to make the latent sample’s source domain identity indistinguishable [16, 23, 30]. It has been shown that too strong of a latent domain matching penalty can harm performance, especially when source domains are unrelated to each other [33] or suffer from label shift [31]. To account for this issue, several techniques have been developed for relaxing the latent domain matching penalty using other objective loss functions [23] or by explicitly re-weighting the importance of matching domains through Multiple Domain Matching Networks (MDMN) [29]. MDMN uses a Wasserstein distance approximation to dynamically re-weight the importance of domain matching depending on the proximity of domains, choosing to use only the

most relevant source domains. While these methods leverage advanced domain adaptation techniques, it is crucial in our situation to also examine the within-domain differences in treatment assignment.

In summary, existing work only partially solves the problem of predicting out-of-domain treatment effects with data from multiple sources.

3 Problem Setup

Suppose we have data from S domains (centers). Let $\{1, \dots, S-1\}$ represent source domains, and let S represent the unobserved target domain. We assume a binary treatment condition with label $T \in \{0, 1\}$. The feature space and the potential outcome space are represented as $X \in \mathcal{X} \subset \mathbb{R}^{p_x}$ and $\{Y(0), Y(1)\} \in \mathcal{Y} \subset \mathbb{R}^{p_y}$, respectively. For any domain s , the selection bias in observational studies causes X to have distinct distributions in the control group ($T = 0$), treatment group ($T = 1$), and overall domain.

$$\text{Control: } X|_{T=0} \sim D_{s,0}; \text{ Treatment: } X|_{T=1} \sim D_{s,1}; \text{ Overall: } X \sim D_s.$$

We use $D_{s,0}$, $D_{s,1}$, and D_s to represent their distribution functions, and their relationship can be described by $(1 - p_s^{T=1})D_{s,0} + p_s^{T=1}D_{s,1} = D_s$, with $p_s^{T=1}$ indicating the marginal probability of treatment assignment. Likewise, $\{g_{s,0}, g_{s,1}\}$ represents the unknown outcome functions for $\{Y(0), Y(1)\}$.

The observable information of an individual data sample of any source domain s is represented via a tuple, $\{T, X, Y = Y(T)\}$. Given a target domain S with $X \sim D_S$, our goal is to accurately infer both potential outcomes, so that we can more accurately estimate treatment outcomes and therefore assign individuals to the treatments that are likely to benefit them most.

There are two obstacles that are likely to hurt generalization to the target domain. The first is selection bias, since treatment assignment is often not randomized in observational studies. As a result, the acquired samples on which the model is trained cannot objectively reflect the error on the full domain, as $D_{s,0} \neq D_{s,1} \neq D_s, \forall s$. The second consideration is domain-level discrepancies, which may inhibit the effects of reducing the error over the combined source domains. More formally, for different domains a and b , we could describe the discrepancies as the shifts in feature space distributions and underlying outcome functions, represented as, $D_a \neq D_b$ and $\{g_{a,0}, g_{a,1}\} \neq \{g_{b,0}, g_{b,1}\}$, respectively. Here, we make similar assumptions to those made in the causal literature [21, 37]; however, we make modifications that account for the extension to our multi-domain scenario.

Assumption 1 (Within-domain positivity). *For domain s where $X \sim D_s$, the probability of assignment to any treatment group is bounded away from zero: $0 < \Pr(T = 1|X, s) < 1$.*

Assumption 2 (Within-domain consistency). *For domain s , the observed outcome with assigned treatment is equal to its potential outcome: $Y|T, X \sim D_s = Y(T)|T, X \sim D_s$.*

Assumption 3 (Within-domain ignorability). *For domain s , the potential outcomes are jointly independent of the treatment assignment conditional on X : $[Y(0), Y(1)] \perp T|X \sim D_s$.*

Considering treatment assignment as probabilistic ensures that studying the treatment difference forms a meaningful target for each domain. The original assumption does not involve s . This could create a problem where the treatment assignment is probabilistic overall ($0 < \Pr(T = 1|X) < 1$) but deterministic at domain level ($\Pr(T = 1|X, s) = 1$ or $\Pr(T = 1|X, s) = 0$). Assumptions 2 and 3 are now also stated *with respects to each domain* to better account for differences at the domain level. As a result, individuals with identical features but from different domains may have treatment assignments and responses that are domain-dependent and thus different overall.

4 Multiple Domain Causal Networks

Multiple Domain Causal Networks (MDCN) is a novel framework that both addresses selection bias in treatment assignment and leverages similarity from different centers. MDCN has three main components, all implemented as neural networks: a feature embedding network $\phi : \mathbb{R}^{p_x} \rightarrow \mathbb{R}^q$ that learns new representations, and two outcome networks $h_0 : \mathbb{R}^q \rightarrow \mathbb{R}$ and $h_1 : \mathbb{R}^q \rightarrow \mathbb{R}$ that infer potential outcomes. The roles of these three components are depicted in Figure 1. Using the taxonomy in Künzel et al. [27], our outcome networks can be considered as a ‘‘T-learner’’.

First, the original feature space X is embedded in $\phi(X)$. This embedding is incorporated into three loss terms, the purpose of each being to endow it with specific properties. Through $L(\phi, h_0, h_1)$, ϕ is injected with information predictive of the outcomes. $L_{BT}(\phi)$ and $L_{CD}(\phi)$ are two regularization terms. The former makes ϕ more robust against the selection bias between treatment groups, and the latter reduces the cross-domain differences so that generalization is improved by learning from examples from similar domains.

$$L_{all}(\phi, h_0, h_1) = L(\phi, h_0, h_1) + \alpha L_{BT}(\phi) + \beta L_{CD}(\phi) \quad (1)$$

The full loss is summarized in (1), with α and β as tuning parameters. In all our experiments, we fix $\alpha = 5e-4$ and $\beta = 1e-3$, as chosen from the range of recommended values in Shalit et al. [41] and Li et al. [29]. Our model has empirically robust performance with these values, although they could be tuned in practice. We give the form of $L(\phi, h_0, h_1)$ below. The design of L_{BT} and L_{CD} are explained in Sections 4.1 and 4.2. $L(\phi, h_0, h_1)$ trains the potential outcome models h_0 and h_1 to predict the observed outcomes given their assigned treatments. We use $l(\cdot, \cdot)$ to represent an arbitrary loss function, the form of which can be chosen based on the requirements of the modeling problem (e.g., cross-entropy loss for binary or categorical outcomes, squared loss for continuous outcomes). (2) represents the expectation of this loss as a summation over all source domains,

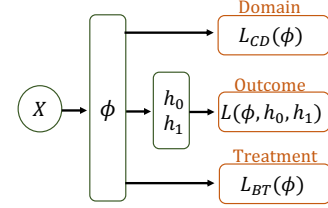


Figure 1: MDCN, ϕ, h_0, h_1 are optimized together with respective losses.

$$L(\phi, h_0, h_1) = \sum_{s=1}^{S-1} \left[E_{x \sim D_{s,0}, y, t} l(h_0(\phi(x), y(t=0))) + E_{x \sim D_{s,1}, y, t} l(h_1(\phi(x), y(t=1))) \right] \quad (2)$$

We note that h_0 and h_1 are used to predict the potential outcomes universally across all domains. This strategy is more scalable compared to the alternative of learning a unique function for each domain. Additionally, we believe that when given enough capacity, h_0 and h_1 can still discern the differences at the domain level when combined with the extra properties endowed in ϕ learned via the losses L_{BT} and L_{CD} . However, when we have a small number of domains, we could construct domain-specific $h_{0,s}$ and $h_{1,s}$. The prediction on the target domain could be based on a weighted summation of the outcome functions from its neighboring sources domains. We also view it as a future goal of varying the design of the potential outcome functions. In Appendix B.1, Algorithm 1 describes the pseudo-code for the full implementation.

4.1 Between-Treatment Adjustment

Our approach to between-treatment adjustment is motivated by counterfactual regression (CFR) [41]. An embedding $\phi(x)$ with increased overlap between different treatment groups is learned to reduce the effects of selection bias, as supported by the theory of Ben-David et al. [6] that generalization between more similar spaces have a lower error bound. To measure and encourage this overlap, we penalize with the Kantorovich-Rubinstein form of the Wasserstein-1 distance [51].

$$\sup_{\|f_{bt}\|_L \leq 1} \mathbb{E}_{x \sim D_0} [f_{bt}(\phi(x))] - \mathbb{E}_{x \sim D_1} [f_{bt}(\phi(x))] \quad (3)$$

D_0 and D_1 in (3) characterize how X is distributed on the treatment group and control group. f_{bt} is drawn from the family of Lipschitz functions with constant 1, which can be approximated by neural networks with a gradient penalty [19]. Through this objective, $\phi(x)$ will be encouraged to reduce the distance between-treatment groups. However, this only resolves the imbalance within a single domain. The direct application of CFR to balance all samples does not address the difficulties inherent to data collected from multiple domains. While overall balance is encouraged and enforced, the balancing of specific domains may be neglected. Moreover, the relative closeness of domains in the original space could also become distorted with this crude adjustment. As a modification, we adopt a separate f_{bt}^s for each domain. This aims at reducing the distance between-treatment groups for *all* domains. As f_{bt}^s is domain-specific, the resulting adjustment is therefore also domain-specific. Additionally, there is less impact on cross-domain relationships. In Section 6.1, we provide visualizations to showcase the advantage of this approach over CFR. With this new strategy, the between group loss is,

$$L_{BT}(\phi, f_{bt}) = \sum_{s=1}^{S-1} \left[\sup_{\|f_{bt}^s\|_L \leq 1} \mathbb{E}_{x \sim D_{i,0}} [f_{bt}^s(\phi(x))] - \mathbb{E}_{x \sim D_{i,1}} [f_{bt}^s(\phi(x))] \right]. \quad (4)$$

We represent $L_{BT}(\phi, f_{cd})$ with notation $L_{BT}(\phi)$, as f_{bt} is an auxiliary function to learn distances. We combine $f_{bt} = \{f_{bt}^1, \dots, f_{bt}^{S-1}\}$ using a single neural network with $S - 1$ outputs, which saves computational cost and encourages information sharing between domains, and use the methods of Gulrajani et al. [19] for learning.

4.2 Cross-Domain Adjustment

We implement a cross-domain adjustment to encourage similarities at the domain level. This is achieved by extending the Multiple Domain Matching Network (MDMN) [29]. Akin to the between-treatment adjustment, we measure and reduce the distance based on the Wasserstein-1 distance. Instead of enforcing the distance penalty statically between any two domains, MDMN adopts a weighting scheme which assigns larger weight to more similar domains in (5). For domains that are far apart or dissimilar, forcefully reducing their differences may result in excessive loss of predictive information. As part of the predictive information is shared by all domains, the rest may be specific to only a few. The domain-specific information is reflected by these differences, which cannot be covered by the domain-invariant representation alone but is helpful in capturing the shift in outcome functions. Therefore, smaller weights are allocated in these instances. Ideally, each domain is matched to a few highly-correlated domains in space and forms clusters. For any domain s , this is formulated as,

$$d(D_s, D_{/s}) = \sup_{\|f_{cd}^s\|_L \leq 1} \mathbb{E}_{x \sim D_s} [f_{cd}^s(\phi(x))] - \sum_{i \neq s} \mathbb{E}_{x \sim D_i} [w_{s,i} f_{cd}^s(\phi(x))]. \quad (5)$$

Specifically, the weight $w_{s,i}$ is calculated according to the pairwise differences between any two domains in (6), and $\sum_{i \neq s} w_{s,i} = 1$. While this distance is minimized by picking the single closest domain, we encourage robustness by smoothing over nearby domains. The weighted summation of all other domains can be seen as a pseudo domain, $D_{/s}$, with the well-defined distribution, $D_{/s} = \sum_{i \neq s} w_{s,i} D_i$:

$$\begin{aligned} \mathbf{l}_s &= \{l_{s,i}\}_{i \neq s}, \quad l_{s,i} = \mathbb{E}_{x \sim D_s} [f_{cd}^s(\phi(x))] - \mathbb{E}_{x \sim D_i} [f_{cd}^s(\phi(x))], \\ \mathbf{w}_s &= \{w_{s,i}\}_{i \neq s} = \text{softmax}(-\mathbf{l}_s). \end{aligned} \quad (6)$$

In practice, \mathbf{l}_s is often accompanied with a temperature term to increase its stability. \mathbf{l}_s at t 'th iteration could be represented as: $\mathbf{l}_s^t = .9\mathbf{l}_s^{t-1} + .1\mathbf{l}_s^c$, with \mathbf{l}_s^c being the estimates from the current batch [29]. Aggregating over all domains gives us the cross domain adjustment term:

$$L_{CD}(\phi, f_{cd}) = \sum_{s=1}^S \left[\sup_{\|f_{cd}^s\|_L \leq 1} \mathbb{E}_{x \sim D_s} [f_{cd}^s(\phi(x))] - \sum_{i \neq s} \mathbb{E}_{x \sim D_i} [w_{s,i} f_{cd}^s(\phi(x))] \right]. \quad (7)$$

Likewise, we can also use notation $L_{CD}(\phi)$ for $L_{CD}(\phi, f_{cd})$. To control for the computational cost, we implement $f_{cd} = \{f_{cd}^1, \dots, f_{cd}^S\}$ in the form of a multi-output function. However, due to the pairwise comparisons in weight calculation, the complexity $\mathcal{O}(S^2)$ is needed as S increases. We train this loss and between-treatment adjustment simultaneously on ϕ again using the gradient penalties of Gulrajani et al. [19], which is depicted in Figure 2.

5 Theoretical Analysis

Here, we provide theoretical analyses to explain the design of MDCN. The overarching goal is to bound the error on the unlabeled target domain via labeled source domain data. Full proofs for the theoretical results presented in this section can be found in Appendix A. We give a few preliminaries below before presenting the final bound. To quantify the difference between hypothesis (or outcome) functions, we state the probabilistic discrepancy defined in Li et al. [29]:

Definition 1 (Probabilistic discrepancy). *For two hypotheses h and $h' : \mathbb{R}^P \rightarrow \mathbb{R}$, their difference given a probabilistic distribution D over \mathcal{X} is defined as $\gamma(h, h'|D) = \mathbb{E}_{x \sim D} |h(x) - h'(x)|$.*

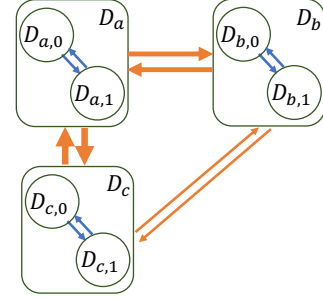


Figure 2: Depiction of cross-domain adjustment with three domains. Wider arrows indicate larger weights/stronger relationships for similar domains.

Next, we define a family of our hypothesis functions in Definition 2. We limit our proposed hypothesis class to the Lipschitz family with parameter λ . $\{h_0, h_1\} \in F_\lambda$.

Definition 2 (Lipschitz continuity). *A function $f : \mathbb{R}^P \rightarrow \mathbb{R}$ is Lipschitz continuous with parameter λ if $|f(x_1) - f(x_2)| \leq \lambda \|x_1 - x_2\|_2$ holds for any vectors $x_1, x_2 \in \mathcal{X}$. We denote the family as \mathcal{F}_λ .*

We assume that the true outcome functions are also included in this family but with a different smoothness parameter λ^* , $\{g_{s,0}, g_{s,1}\}_{s=1}^S \in F_{\lambda^*}$. This encourages smooth transitions in the outcome labels with regards to changes in the feature space. Though smoothness may not hold in practice, Lipschitz continuous functions provide a reasonable approximation to a wide range of functions [44]. With all the preliminaries, we can present the overall bound on the target domain in Theorem 1,

Theorem 1. *For any positive weights $w = \{w_s\}_{s=1}^{S-1}$ with $\sum_{s=1}^{S-1} w_s = 1$, the discrepancy between the true hypothesis functions $\{g_{0,S}, g_{1,S}\}$ and the proposed hypothesis functions $\{h_0, h_1\}$ on target domain S is bounded by,*

$$\begin{aligned} \gamma(h_0, g_{s,0}|D_S) + \gamma(h_1, g_{s,1}|D_S) &\leq (\lambda + \lambda^*)[2W_1(D_S, \sum_{s=1}^{S-1} w_s D_s) + \sum_{s=1}^{S-1} w_s W_1(D_{s,0}, D_{s,1})] \\ &+ \sum_{s=1}^{S-1} w_s [\gamma(h_0, g_{s,0}|D_{s,0}) + \gamma(h_1, g_{s,1}|D_{s,1})] + \gamma_0^* + \gamma_1^*. \end{aligned} \quad (8)$$

$[\gamma(h_0, g_{s,0}|D_{s,0}) + \gamma(h_1, g_{s,1}|D_{s,1})]$ represents the probabilistic discrepancy between $\{h_0, h_1\}$ and the true outcome functions $\{g_{s,0}, g_{s,1}\}$ on the observable part of the data: $D_{s,0}, D_{s,1}$. Minimizing this corresponds to $L(\phi, h_0, h_1)$ in (2). In practice, we could modify the discrepancy mildly such as by optimizing the squared loss in regressions instead for more stability. $W_1(D_{s,0}, D_{s,1})$ measures the distance between the treatment space and the control space in domain s , and it matches with the structure of $L_{BC}(\phi)$. Likewise, $L_{CD}(\phi)$ is inspired by $W_1(D_S, \sum_{s=1}^{S-1} w_s D_s)$. Though the bound is dependent on the values of λ or λ^* , their explicit values are not needed in practice, as they can be incorporated into tuning parameters α and β . Lastly, $\gamma_0^* + \gamma_1^*$ depicts the fundamental difference in the true outcome functions $\{g_{s,0}, g_{s,1}\}_{s=1}^S$ across domains, and cannot be optimized. A large $\gamma_0^* + \gamma_1^*$ signals the existence of a huge shift in outcome functions. In that case, we are less guaranteed to achieve accurate predictions on the target domain. The weight $w = \{w_s\}_{s=1}^{S-1}$ also plays a key role in this bound. In (8), increased emphasis is placed on source domains that are close to the target domain. Samples from these similar source domains may serve as good reference cases and provide valuable insights in improving the performance on the target domain.

6 Experiments

We use two examples to demonstrate how MDCN improves estimation of heterogeneous treatment effects on the target domain. Efficacy is evaluated according to estimation of the conditional average treatment effect (CATE) [41]. We modify CATE by conditioning the quality on the domain label S to take into consideration the shift in outcome functions:

$$\tau(x, S) = \mathbb{E}[Y(1)|x, S] - \mathbb{E}[Y(0)|x, S]. \quad (9)$$

We use the precision in estimation of heterogeneous treatment effects (PEHE) from Hill [22] to measure the distance between CATE and its estimates: $\text{PEHE}(S) = \sqrt{\mathbb{E}_{x \sim D_S} [\tau(x, S) - \hat{\tau}(x, S)]^2}$. As evaluating CATE requires access to ground truth values, we create synthetic and semi-synthetic data for this purpose. Causal forest (CF) is included as a benchmark due to its previous application to multicenter observational study data [2, 46]. Other benchmarks include different variants of MDCN, which also serves as an ablation study that helps us understand the benefits of different components of MDCN. Apart from CF, we note that all variants have identical architectures for the outcome model and feature embedding model to ensure a fair comparison. CFR is included as a naïve benchmark that only addresses treatment group imbalance globally [41]. The proposed between-treatment adjustment $L_{BT}(\phi)$ in (4) upgrades CFR by performing the novel adjustment *within* each domain, which we call the domain CFR (DCFR). Performance of MDMN is also compared to illustrate the inadequacy of applying the domain-level adjustment alone. Lastly, we combine MDMN and CFR to form MDMNCFR. Though it adjusts at both cross-domain and between-treatment levels, its design is inferior to MDCN which is rigorously backed by supporting theories. Additional details can be found in Appendix B.1.

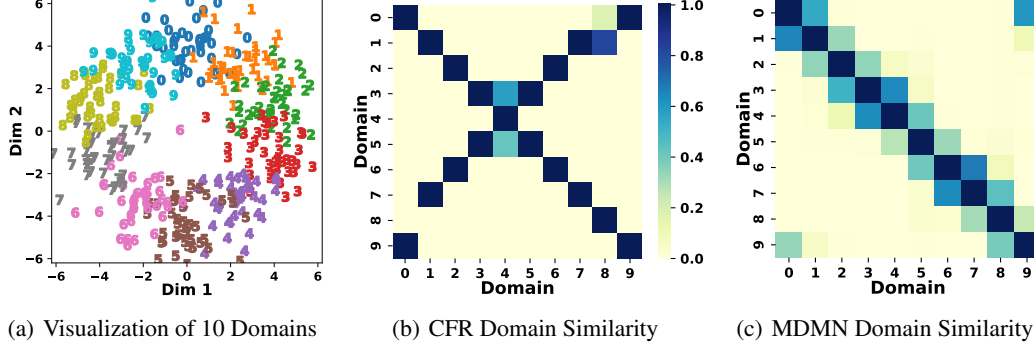


Figure 3: 3(a) visualizes the locations of the 10 domains. 3(b) and 3(c) are the heat maps measuring the similarity between domains. For MDMN-based approaches (MDCN included), we use the learned weight $(w_{s',s} + w_{s,s'})/2$ to fill in the grid s, s' . For other methods, we use $\phi(x)$'s 1d t-SNE [32] to estimate the distance l_s and weight w_s in (6) to plot the similarity (details in Appendix C). Darker colors indicate more similarity. Ideally, the whole diagonal and two off-diagonal corners should be dark with more decaying for grids further away from them. CFR strongly connects some distant domains, such as 1 and 7 or 2 and 6. Essentially, it reduces the distances in the diagonal to reduce the treatment group imbalance marginally, which contradicts with how similarity is shared between near domains. MDCN fully recovers the true similarity. Other methods are visualized in Figure S1.

6.1 Synthetic Circular Data

In this section, we create a synthetic case with shifts in both feature spaces and outcome functions across domains. We define the dimension of the feature space $\mathcal{X} \in \mathbb{R}^3$ and the number of domains $S = 10$. These domains are labeled by $s \in \{0, \dots, 9\}$. Any domain s versus the rest of the combined domains can be regarded as the setup for source versus target domains. To simulate the data, we first use s to create an angle parameter: $\angle_s = s \times \pi/10$, which evenly splits a circle. Through \angle_s , we vary domains and outcome functions with the following procedures.

$$\begin{aligned}
 \text{Domain shift:} \quad & X|s = \{x_1, x_2, x_3\} \sim \mathcal{N}([4 \sin(\angle_s), 4 \cos(\angle_s), 0]', \mathbb{I}_3); \\
 \text{Potential outcomes:} \quad & Y(0)|X, s \sim \mathcal{N}(1.5[\sin(x_1 + \angle_s) + \cos(x_2 + x_3 + \angle_s)], 1), \\
 & Y(1)|X, s \sim \mathcal{N}(1.5[\cos(x_1 + \angle_s) + \sin(x_2 + x_3 + \angle_s)], 1); \\
 \text{Treatment Assignment :} \quad & \mathbb{P}(T = 1|X) = 1/[1 + \exp(-0.5x_1 - 0.5x_2 - 2x_3)].
 \end{aligned}$$

For source domains, the observed outcomes correspond to the outcomes with assigned treatments $Y = Y(0)(1 - T) + Y(1)T$. We simulate 2,000 samples for each domain and repeat this procedure 10 times for variability assessment. The distributions for 10 domains in their first two dimensions are visualized in Figure 3(a). The location shift of 10 domains forms a circle, and each domain s has 2 close neighbors on its two sides with labels: $s - 1 \pmod{10}$ and $s + 1 \pmod{10}$.

The results on PEHE are summarized in Table 1. For lower dimensional manifolds, tree-based approaches are advantageous as samples can easily saturate the space. However, CF lacks the structure to address the shifts in domains and outcome functions, so it only slightly outperforms MLP. Compared with MLP, other methods with adjustments demonstrate clear improvements in accuracy. DCFR minimizes the treatment imbalance within each domain instead of marginally like CFR. This lessens the impact of domain-level relationships, thus resulting in better performance. This result is visualized in Figure 3(b), as CFR distorts some of the cross-domain similarities to alleviate the marginal treatment imbalance (e.g., regarding domain 2 and 6 to be closely connected). DCFR visualized in S1 better maintains the original domain-level connectivity. MDCM in Figure 4(c) can clearly recover the true similarity. The combination of CFR and MDMN (MDNMCFR) does not improve MDMN. MDCN has a clear advantage over all other benchmarks, achieving top marks in 5 out of 10 domains as well as best overall performance.

Table 1: PEHE on Circular Data. MDMN is the most competitive of all benchmarks. Adjusting treatment group imbalance within each domain (DCFR) consistently outperforms CFR in all domains. Wilcoxon signed-rank test is used to report the significance between our newly proposed approaches and CFR. P value $< 5 \cdot 10^{-2}$ (\dagger), P value $< 1 \cdot 10^{-4}$ ($\dagger\dagger$).

Target Domain	CF	MLP	CFR	MDMN	MDMNCFR $\dagger\dagger$	DCFR $\dagger\dagger$	MDCN $\dagger\dagger$
0	1.24 \pm .02	1.69 \pm .08	1.59 \pm .07	1.31 \pm .05	1.33 \pm .05	1.37 \pm .07	1.28 \pm .07
1	2.55 \pm .03	2.01 \pm .05	1.99 \pm .08	1.42 \pm .04	1.34 \pm .04	1.48 \pm .09	1.37 \pm .04
2	1.43 \pm .03	1.33 \pm .06	1.32 \pm .03	1.16 \pm .04	1.17 \pm .05	1.19 \pm .03	1.18 \pm .04
3	1.44 \pm .03	1.27 \pm .04	1.25 \pm .03	1.01 \pm .04	1.00 \pm .03	1.02 \pm .02	0.99 \pm .03
4	1.45 \pm .01	1.31 \pm .06	1.29 \pm .05	1.20 \pm .02	1.23 \pm .03	1.19 \pm .04	1.16 \pm .03
5	1.52 \pm .02	1.34 \pm .07	1.25 \pm .05	1.28 \pm .05	1.31 \pm .08	1.25 \pm .06	1.24 \pm .07
6	1.41 \pm .03	1.47 \pm .07	1.32 \pm .06	1.34 \pm .07	1.26 \pm .02	1.25 \pm .03	1.32 \pm .05
7	2.20 \pm .02	1.82 \pm .08	1.87 \pm .12	1.64 \pm .10	1.80 \pm .07	1.49 \pm .07	1.60 \pm .06
8	1.69 \pm .03	2.15 \pm .05	2.10 \pm .07	1.69 \pm .04	1.71 \pm .04	1.65 \pm .07	1.62 \pm .04
9	1.49 \pm .03	2.17 \pm .07	2.31 \pm .08	1.65 \pm .06	1.59 \pm .08	1.61 \pm .09	1.49 \pm .06
Overall	1.64 \pm .04	1.66 \pm .04	1.63 \pm .04	1.37 \pm .03	1.37 \pm .03	1.35 \pm .03	1.33 \pm .03

Table 2: PEHE on Mice Data. MDCN gives the overall best performance, and is the best approach in 9 out of 21 domains. P value $< 5 \cdot 10^{-2}$ (\dagger), P value $< 1 \cdot 10^{-4}$ ($\dagger\dagger$).

Target Domain	CF	MLP	CFR	MDMN	MDMNCFR \dagger	DCFR $\dagger\dagger$	MDCN $\dagger\dagger$
0	7.64 \pm .07	1.61 \pm .02	1.50 \pm .02	1.52 \pm .05	1.56 \pm .04	1.45 \pm .06	1.52 \pm .06
1	3.73 \pm .06	4.21 \pm .12	4.12 \pm .12	3.31 \pm .19	3.35 \pm .09	3.24 \pm .12	3.45 \pm .08
2	5.17 \pm .04	5.42 \pm .11	4.94 \pm .13	3.29 \pm .16	3.95 \pm .26	3.70 \pm .20	3.15 \pm .23
3	6.92 \pm .04	2.07 \pm .05	2.11 \pm .05	2.01 \pm .07	2.16 \pm .05	2.10 \pm .06	2.17 \pm .07
4	4.09 \pm .12	2.61 \pm .07	2.47 \pm .06	2.57 \pm .08	2.68 \pm .10	2.65 \pm .08	2.63 \pm .07
5	6.68 \pm .04	1.49 \pm .12	1.37 \pm .08	1.39 \pm .03	1.34 \pm .05	1.31 \pm .04	1.40 \pm .07
6	3.77 \pm .05	2.19 \pm .06	2.40 \pm .14	2.26 \pm .06	2.26 \pm .06	2.33 \pm .08	2.26 \pm .08
7	6.06 \pm .21	4.85 \pm .08	5.11 \pm .07	5.20 \pm .08	5.22 \pm .10	5.27 \pm .09	5.11 \pm .05
8	2.84 \pm .05	2.27 \pm .10	2.23 \pm .10	1.71 \pm .11	1.87 \pm .17	1.73 \pm .10	1.70 \pm .09
9	2.53 \pm .11	1.88 \pm .16	1.76 \pm .15	2.04 \pm .22	1.57 \pm .14	1.48 \pm .14	1.31 \pm .07
10	4.54 \pm .25	1.72 \pm .10	1.50 \pm .08	1.46 \pm .05	1.50 \pm .03	1.40 \pm .06	1.41 \pm .03
11	7.54 \pm .16	1.66 \pm .03	1.72 \pm .08	1.44 \pm .07	1.41 \pm .05	1.38 \pm .06	1.24 \pm .04
12	2.70 \pm .14	2.81 \pm .13	2.79 \pm .08	2.90 \pm .11	2.99 \pm .08	2.87 \pm .09	2.96 \pm .10
13	2.60 \pm .06	1.67 \pm .19	1.56 \pm .12	1.98 \pm .12	2.26 \pm .18	1.91 \pm .15	2.23 \pm .24
14	4.40 \pm .42	1.48 \pm .02	1.38 \pm .02	1.39 \pm .02	1.47 \pm .02	1.43 \pm .03	1.43 \pm .03
15	2.49 \pm .15	3.20 \pm .15	2.95 \pm .13	2.38 \pm .11	2.37 \pm .10	2.47 \pm .14	2.54 \pm .11
16	3.62 \pm .17	2.66 \pm .03	2.51 \pm .13	2.60 \pm .17	2.34 \pm .09	2.46 \pm .12	2.21 \pm .09
17	2.66 \pm .44	1.68 \pm .03	1.57 \pm .02	1.59 \pm .05	1.51 \pm .02	1.55 \pm .05	1.51 \pm .03
18	5.84 \pm .17	6.14 \pm .20	5.95 \pm .16	4.90 \pm .34	5.12 \pm .23	5.17 \pm .38	4.75 \pm .27
19	4.42 \pm .24	2.03 \pm .07	1.81 \pm .07	1.41 \pm .05	1.41 \pm .05	1.38 \pm .03	1.37 \pm .05
20	2.29 \pm .15	2.49 \pm .09	2.36 \pm .12	2.38 \pm .10	2.28 \pm .09	2.29 \pm .08	2.28 \pm .09
overall	4.41 \pm .13	2.77 \pm .09	2.58 \pm .09	2.37 \pm .08	2.41 \pm .08	2.36 \pm .08	2.32 \pm .07

6.2 Semi-Synthetic Mouse Data

In this experiment, we make use of a mouse local field potential (LFP) dataset collected in Gallagher et al. [15]. These data were collected from 21 mice in accordance with guidelines provided by the Institutional Animal Care and Use Committee (IACUC). LFPs were recorded while each mouse was exposed to two conditions: “home cage” (resting state, low stress) and “open field” (mild increased stress) [5]. We use these two states to mimic the control (home cage) and treatment (open field) groups, thus providing an analog to multicenter observational study data. Individual mice, similarly to individual sites, are expected to demonstrate heterogeneity. We define an observation as each 1 second-long window of brain signal recordings which is associated with a continuous outcome, such as a behavioral outcome. Each mouse has less than 500 observations for each state. This treatment structure mimics approaches in closed-loop brain stimulation, which chooses treatments based on current neural representations, and is currently in use in depression [39] and seizure prevention [45].

Features meant to capture neural dynamics are generated from LFP data, including power spectral density [52], coherence, and Granger causality [18] for a total of with 9,856 features. To artificially increase sample size, we employ an auto-encoder method that simultaneously interpolates the space between samples and reduces dimensionality [35]. Further experimental details are provided in Appendix B.2. Following preprocessing, each domain contains 20,000 samples with the feature space dimension reduced to a dimensionality 15. The new feature space still retains domain-specific information, as mouse identity can be accurately predicted ($> 90\%$). Next, we simulate the potential outcomes. We randomly draw 15 correlated neural networks with the input and output size: $\mathbb{R}^{15} \rightarrow \mathbb{R}$,

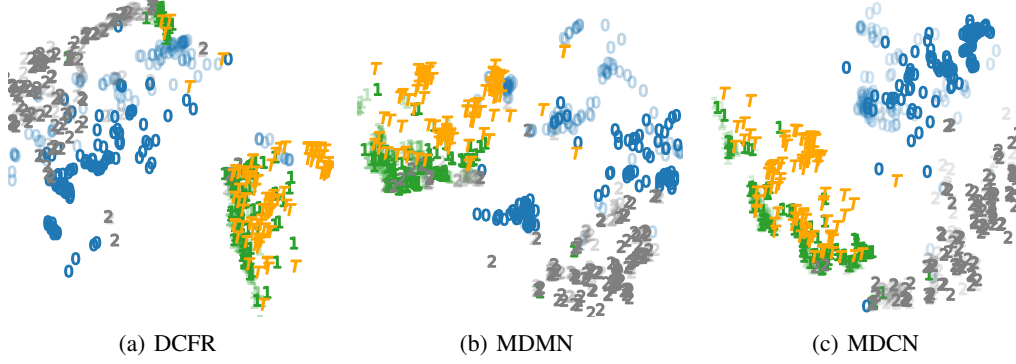


Figure 4: T-SNE plot of $\phi(x)$. The domain 9 is chosen as the target domain and indicated with an orange "T". For convenience, the three nearest neighbors of the target domain are labeled as "0", "1", and "2". The weight matrix in MDCN and MDMN both identify the same three neighbors. Solid transparent shades represent the control and treatment groups, respectively. In 4(a), the target domain lies on the outer perimeter of these three neighbors indicating lesser similarity. In 4(b), there exists a visible separation between the treatment and the control groups in the neighbor "0". In 4(c), MDCN balances the treatment and control groups with respects to its neighbors, and the target domain is properly surrounded by the three neighbors. Other visualizations are provided in Appendix C.

for both states, $\{f_1^0, \dots, f_{15}^0\}, \{f_1^1, \dots, f_{15}^1\}$, that are designed to vary with the center of each domain s , $\bar{x}^s = \{\bar{x}_1^s, \dots, \bar{x}_{15}^s\}$ (details provided in Appendix B.2). Essentially, domains that are close in center tend to have similar outcome functions. We simulate the potential outcomes for domain s as follows, $Y(0)|X, s \sim \mathcal{N}(\sum_{j=1}^{15} \sigma(\bar{x}_1^s) f_j^0(X), 1)$; $Y(1)|X, s \sim \mathcal{N}(\sum_{j=1}^{15} \sigma(\bar{x}_1^s) f_j^1(X), 1)$.

We evenly split the data into 10 folds for variability assessment with results summarized in Table 2. The drawbacks of the tree-based CF approach are demonstrated as the increased feature dimension exacerbates decrease of domain overlap. MDCN demonstrates the best performance in 9 domains, outperforming benchmarks which conduct either domain-level adjustment (MDMN) or treatment-level adjustment (DCFR) but not both. DCFR outperforms CFR with statistical significance, which further supports adjusting for treatment imbalance differentially in different domains. This is also reflected in the combination of CFR and MDMN (MDMNCFR), which results in a drop in performance when compared to MDMN. We visualize the learned feature embeddings $\phi(x)$ in Figure S2, shedding light on how MDCN predicts on unlabeled target domains. We first find the three closest "neighborhoods" to the target domain using the MDCN weight matrix and then plot their relative positions. The target domain in MDCN is located at the center of its three neighbors in Figure 4(c), which enables it to borrow information from their respective outcome predictions. Additionally, the treatment and control groups from the three neighbors are all well-balanced, making MDCN more robust against treatment group imbalances. In Figure 4(a), DCFR regards two of its neighbors as irrelevant domains, preventing it from learning from more reference cases. In Figure 4(b), the treatment group imbalance is not well controlled in MDMN, thus resulting in less competitive generalization to the target domain.

7 Discussion

Here, we propose MDCN, an approach that provides robust estimation of the conditional treatment effect for data collected from multi-center observational studies with particular emphasis in accurately inferring treatment effects from individuals from a new center. Our approach addresses a lack of methods research with respects to this specific but not uncommon problem. More importantly, our model demonstrates the potential to provide patients from new, unobserved centers with better references for treatment. Additionally, we also elaborate on the design of MDCN and underpin it with supporting theory. In empirical evaluations, MDCN consistently outperforms state-of-the-art domain adaptation methods and causal methods. One limitation of MDCN lies in the scalability with respects to domain size S which comes at a cost of $\mathcal{O}(S^2)$. To address this scalability issue, one could combine similar domains via some similarity heuristic. Likewise, scalability becomes an issue when

handling multiple or continuous treatment regimes. As the number of treatment groups increases, learning a balanced treatment embedding tends to be more challenging. Adequately addressing these issues provides interesting directions for future research in this area. Moving forward, our techniques may be applied to multicenter observational studies and neuromodulation; the ethics of neuromodulation are complex, and we do not view our study as directly impacting these discussions. Finally, as with any developed methodology with relevance to healthcare, the methods proposed here should not be solely relied upon to guide clinical practice, suggest treatments, or recommend any health-related actions without consultation and close collaboration with medical professionals.

Acknowledgments

Research reported in this manuscript was supported by the National Institute of Biomedical Imaging and Bioengineering and the National Institute of Mental Health through the National Institutes of Health BRAIN Initiative under Award Number R01EB026937 and the National Institute Of Mental Health of the National Institutes of Health under Award Number R01MH125430. The content is solely the responsibility of the authors and does not necessarily represent the official views of the National Institutes of Health.

References

- [1] Serge Assaad, Shuxi Zeng, Chenyang Tao, Shounak Datta, Nikhil Mehta, Ricardo Henao, Fan Li, and Lawrence Carin. Counterfactual representation learning with balancing weights. *Artificial Intelligence and Statistics*, 2021.
- [2] Susan Athey and Guido Imbens. Recursive partitioning for heterogeneous causal effects. *Proceedings of the National Academy of Sciences*, 113(27):7353–7360, 2016.
- [3] Usaid Awan, Marco Morucci, Vittorio Orlandi, Sudeepa Roy, Cynthia Rudin, and Alexander Volfovsky. Almost-matching-exactly for treatment effect estimation under network interference. In *International Conference on Artificial Intelligence and Statistics*, pages 3252–3262, 2020.
- [4] Kamyar Azizzadenesheli, Anqi Liu, Fanny Yang, and Animashree Anandkumar. Regularized learning for domain adaptation under label shifts. In *International Conference on Learning Representations*, 2019.
- [5] Kathleen R Bailey and Jacqueline N Crawley. Anxiety-related behaviors in mice. *Methods of Behavior Analysis in Neuroscience*, 2009.
- [6] Shai Ben-David, John Blitzer, Koby Crammer, Alex Kulesza, Fernando Pereira, and Jennifer Wortman Vaughan. A theory of learning from different domains. *Machine Learning*, 79(1-2):151–175, 2010.
- [7] Karsten M. Borgwardt, Arthur Gretton, Malte J. Rasch, Hans-Peter Kriegel, Bernhard Schölkopf, and Alex J. Smola. Integrating structured biological data by kernel maximum mean discrepancy. *Bioinformatics*, 22(14):e49–e57, 2006.
- [8] Yale Chang and Jennifer Dy. Informative subspace learning for counterfactual inference. In *Proceedings of the AAAI Conference on Artificial Intelligence*, volume 31, 2017.
- [9] Rudi De Raedt, Marie-Anne Vanderhasselt, and Chris Baeken. Neurostimulation as an intervention for treatment resistant depression: From research on mechanisms towards targeted neurocognitive strategies. *Clinical Psychology Review*, 41:61–69, 2015.
- [10] Angus Deaton. Instruments, randomization, and learning about development. *Journal of Economic Literature*, 48(2):424–55, 2010.
- [11] Clevert Djork-Arné, Thomas Unterthiner, and Sepp Hochreiter. Fast and accurate deep network learning by exponential linear units (elus). In *Proceedings of the International Conference on Learning Representations*, volume 6, 2016.

- [12] Andrew T Drysdale, Logan Grosenick, Jonathan Downar, Katharine Dunlop, Farrokh Mansouri, Yue Meng, Robert N Fetcho, Benjamin Zebley, Desmond J Oathes, Amit Etkin, et al. Resting-state connectivity biomarkers define neurophysiological subtypes of depression. *Nature Medicine*, 23(1):28–38, 2017.
- [13] Angela Lee Duckworth, Eli Tsukayama, and Henry May. Establishing causality using longitudinal hierarchical linear modeling: An illustration predicting achievement from self-control. *Social Psychological and Personality Science*, 1(4):311–317, 2010.
- [14] Ricard Ferrer, Antonio Artigas, David Suarez, Eduardo Palencia, Mitchell M Levy, Angel Arenzana, Xose Luis Pérez, and Josep-Maria Sirvent. Effectiveness of treatments for severe sepsis: A prospective, multicenter, observational study. *American Journal of Respiratory and Critical Care Medicine*, 180(9):861–866, 2009.
- [15] Neil Gallagher, Kyle R Ulrich, Austin Talbot, Kafui Dzirasa, Lawrence Carin, and David E Carlson. Cross-spectral factor analysis. In I. Guyon, U. Von Luxburg, S. Bengio, H. Wallach, R. Fergus, S. Vishwanathan, and R. Garnett, editors, *Advances in Neural Information Processing Systems*, volume 30, 2017.
- [16] Yaroslav Ganin, Evgeniya Ustinova, Hana Ajakan, Pascal Germain, Hugo Larochelle, François Laviolette, Mario March, and Victor Lempitsky. Domain-adversarial training of neural networks. *Journal of Machine Learning Research*, 17(59):1–35, 2016.
- [17] Xavier Glorot and Yoshua Bengio. Understanding the difficulty of training deep feedforward neural networks. In *Proceedings of the International Conference on Artificial Intelligence and Statistics*, pages 249–256, 2010.
- [18] C. W. J. Granger. Investigating causal relations by econometric models and cross-spectral methods. *Econometrica*, 37(3):424–438, 1969.
- [19] Ishaan Gulrajani, Faruk Ahmed, Martin Arjovsky, Vincent Dumoulin, and Aaron C Courville. Improved training of wasserstein gans. *Advances in Neural Information Processing Systems*, 30, 2017.
- [20] Negar Hassanpour and Russell Greiner. Variational auto-encoder architectures that excel at causal inference. *Advances in Neural Information Processing Systems*, 2020.
- [21] Miguel A Hernan and James M Robins. *Causal Inference*. Boca Raton: Chapman & Hall/CRC, 2020.
- [22] Jennifer L Hill. Bayesian nonparametric modeling for causal inference. *Journal of Computational and Graphical Statistics*, 20(1):217–240, 2011.
- [23] Judy Hoffman, Eric Tzeng, Taesung Park, Jun-Yan Zhu, Phillip Isola, Kate Saenko, Alexei Efros, and Trevor Darrell. CyCADA: Cycle-consistent adversarial domain adaptation. In Jennifer Dy and Andreas Krause, editors, *Proceedings of the International Conference on Machine Learning*, volume 80 of *Proceedings of Machine Learning Research*, pages 1989–1998. PMLR, 2018.
- [24] Kewal K Jain. Personalized medicine. *Current Opinion in Molecular Therapeutics*, 4(6): 548–558, 2002.
- [25] Diederik P Kingma and Jimmy Ba. Adam: A method for stochastic optimization. *Proceedings of the International Conference on Learning Representations*, 2015.
- [26] Kun Kuang, Peng Cui, Bo Li, Meng Jiang, Shiqiang Yang, and Fei Wang. Treatment effect estimation with data-driven variable decomposition. In *Proceedings of the AAAI Conference on Artificial Intelligence*, volume 31, 2017.
- [27] Sören R Künnel, Jasjeet S Sekhon, Peter J Bickel, and Bin Yu. Metalearners for estimating heterogeneous treatment effects using machine learning. *Proceedings of the National Academy of Sciences*, 116(10):4156–4165, 2019.

- [28] Fan Li, Kari Lock Morgan, and Alan M Zaslavsky. Balancing covariates via propensity score weighting. *Journal of the American Statistical Association*, 113(521):390–400, 2018.
- [29] Yitong Li, michael Murias, geraldine Dawson, and David E Carlson. Extracting relationships by multi-domain matching. In S. Bengio, H. Wallach, H. Larochelle, K. Grauman, N. Cesa-Bianchi, and R. Garnett, editors, *Advances in Neural Information Processing Systems*, volume 31. Curran Associates, Inc., 2018.
- [30] Yitong Li, Michael Murias, Samantha Major, Geraldine Dawson, and David Carlson. On target shift in adversarial domain adaptation. In *Proceedings of the Twenty-Second International Conference on Artificial Intelligence and Statistics*, volume 89 of *Proceedings of Machine Learning Research*, pages 616–625, 2019.
- [31] Yitong Li, Michael Murias, Samantha Major, Geraldine Dawson, and David Carlson. On target shift in adversarial domain adaptation. In *International Conference on Artificial Intelligence and Statistics*, pages 616–625. PMLR, 2019.
- [32] Laurens van der Maaten. Visualizing data using t-sne. *Journal of Machine Learning Research*, 9:2579–2605, 2008.
- [33] Yishay Mansour, Mehryar Mohri, and Afshin Rostamizadeh. Domain adaptation with multiple sources. In D. Koller, D. Schuurmans, Y. Bengio, and L. Bottou, editors, *Advances in Neural Information Processing Systems*, volume 21. Curran Associates, Inc., 2008.
- [34] CA McGilchrist. Estimation in generalized mixed models. *Journal of the Royal Statistical Society: Series B (Methodological)*, 56(1):61–69, 1994.
- [35] Alon Oring, Zohar Yakhini, and Yacov Hel-Or. Autoencoder image interpolation by shaping the latent space. In *Proceedings of the International Conference on Machine Learning*, volume 139 of *Proceedings of Machine Learning Research*, pages 8281–8290. PMLR, 2021.
- [36] Russell Reed and Robert J Marks II. *Neural smithing: Supervised learning in feedforward artificial neural networks*. Mit Press, 1999.
- [37] Paul R Rosenbaum and Donald B Rubin. The central role of the propensity score in observational studies for causal effects. *Biometrika*, 70(1):41–55, 1983.
- [38] Donald B Rubin and Neal Thomas. Combining propensity score matching with additional adjustments for prognostic covariates. *Journal of the American Statistical Association*, 95(450): 573–585, 2000.
- [39] Katherine W Scangos, Ankit N Khambhati, Patrick M Daly, Ghassan S Makhoul, Leo P Sugrue, Hashem Zamanian, Tony X Liu, Vikram R Rao, Kristin K Sellers, Heather E Dawes, et al. Closed-loop neuromodulation in an individual with treatment-resistant depression. *Nature medicine*, 27(10):1696–1700, 2021.
- [40] Jürgen Schmidhuber. Deep learning in neural networks: An overview. *Neural Networks*, 61: 85–117, 2015.
- [41] Uri Shalit, Fredrik D Johansson, and David Sontag. Estimating individual treatment effect: generalization bounds and algorithms. In *International Conference on Machine Learning*, pages 3076–3085. PMLR, 2017.
- [42] Jian Shen, Yanru Qu, Weinan Zhang, and Yong Yu. Wasserstein distance guided representation learning for domain adaptation. *Proceedings of the AAAI Conference on Artificial Intelligence*, 32(1), 2018.
- [43] Claudia Shi, David Blei, and Victor Veitch. Adapting neural networks for the estimation of treatment effects. In *Advances in Neural Information Processing Systems*, pages 2507–2517, 2019.
- [44] Houshang H Sohrab. *Basic Real Analysis*, volume 231. Springer, 2003.

- [45] Scott Stanslaski, Pedram Afshar, Peng Cong, Jon Giftakis, Paul Stypulkowski, Dave Carlson, Dave Linde, Dave Ullestad, Al-Thaddeus Avestruz, and Timothy Denison. Design and validation of a fully implantable, chronic, closed-loop neuromodulation device with concurrent sensing and stimulation. *IEEE Transactions on Neural Systems and Rehabilitation Engineering*, 20(4): 410–421, 2012.
- [46] Youmi Suk, Hyunseung Kang, and Jee-Seon Kim. Random forests approach for causal inference with clustered observational data. *Multivariate Behavioral Research*, 56(6):829–852, 2021.
- [47] Baochen Sun and Kate Saenko. Deep coral: Correlation alignment for deep domain adaptation. In Gang Hua and Hervé Jégou, editors, *Computer Vision – ECCV 2016 Workshops*, pages 443–450, Cham, 2016. Springer International Publishing.
- [48] Baochen Sun, Jiashi Feng, and Kate Saenko. Return of frustratingly easy domain adaptation. In *Proceedings of the Thirtieth AAAI Conference on Artificial Intelligence*, page 2058–2065. AAAI Press, 2016.
- [49] Remi Tachet des Combes, Han Zhao, Yu-Xiang Wang, and Geoffrey J Gordon. Domain adaptation with conditional distribution matching and generalized label shift. In H. Larochelle, M. Ranzato, R. Hadsell, M.F. Balcan, and H. Lin, editors, *Advances in Neural Information Processing Systems*, volume 33, pages 19276–19289. Curran Associates, Inc., 2020.
- [50] Julie Tibshirani, Susan Athey, and Stefan Wager. *grf: Generalized Random Forests*, 2020. URL <https://CRAN.R-project.org/package=grf>. R package version 1.2.0.
- [51] Cédric Villani. *Optimal Transport: Old and New*, volume 338. Springer Science & Business Media, 2008.
- [52] P. Welch. The use of fast fourier transform for the estimation of power spectra: A method based on time averaging over short, modified periodograms. *IEEE Transactions on Audio and Electroacoustics*, 15(2):70–73, 1967.
- [53] Guoyi Zhang and Yan Lu. Bias-corrected random forests in regression. *Journal of Applied Statistics*, 39(1):151–160, 2012.
- [54] Kun Zhang, Bernhard Schölkopf, Krikamol Muandet, and Zhikun Wang. Domain adaptation under target and conditional shift. In *Proceedings of the International Conference on International Conference on Machine Learning - Volume 28*, page 819–827, 2013.
- [55] Han Zhao, Remi Tachet Des Combes, Kun Zhang, and Geoffrey Gordon. On learning invariant representations for domain adaptation. In Kamalika Chaudhuri and Ruslan Salakhutdinov, editors, *Proceedings of the International Conference on Machine Learning*, volume 97 of *Proceedings of Machine Learning Research*, pages 7523–7532. PMLR, 2019.

Checklist

1. For all authors...
 - (a) Do the main claims made in the abstract and introduction accurately reflect the paper’s contributions and scope? [\[Yes\]](#)
 - (b) Did you describe the limitations of your work? [\[Yes\]](#) In Section 7.
 - (c) Did you discuss any potential negative societal impacts of your work? [\[Yes\]](#) In Section 7.
 - (d) Have you read the ethics review guidelines and ensured that your paper conforms to them? [\[Yes\]](#)
2. If you are including theoretical results...
 - (a) Did you state the full set of assumptions of all theoretical results? [\[Yes\]](#) In Sections 3, 4 and A.
 - (b) Did you include complete proofs of all theoretical results? [\[Yes\]](#) In Section A.
3. If you ran experiments...

- (a) Did you include the code, data, and instructions needed to reproduce the main experimental results (either in the supplemental material or as a URL)? [\[Yes\]](#) In the supplemental material.
 - (b) Did you specify all the training details (e.g., data splits, hyperparameters, how they were chosen)? [\[Yes\]](#) In Section B.1.
 - (c) Did you report error bars (e.g., with respect to the random seed after running experiments multiple times)? [\[Yes\]](#) In Table 1 and 2.
 - (d) Did you include the total amount of compute and the type of resources used (e.g., type of GPUs, internal cluster, or cloud provider)? [\[Yes\]](#) In Section B.1.
4. If you are using existing assets (e.g., code, data, models) or curating/releasing new assets...
- (a) If your work uses existing assets, did you cite the creators? [\[Yes\]](#) In Section B.1 and 6.2.
 - (b) Did you mention the license of the assets? [\[Yes\]](#) In Section B.1 and 6.2.
 - (c) Did you include any new assets either in the supplemental material or as a URL? [\[Yes\]](#) In the supplemental material.
 - (d) Did you discuss whether and how consent was obtained from people whose data you're using/curating? [\[N/A\]](#) The assets were approved by Institutional Animal Care and Use Committee (IACUC).
 - (e) Did you discuss whether the data you are using/curating contains personally identifiable information or offensive content? [\[N/A\]](#)
5. If you used crowdsourcing or conducted research with human subjects...
- (a) Did you include the full text of instructions given to participants and screenshots, if applicable? [\[N/A\]](#)
 - (b) Did you describe any potential participant risks, with links to Institutional Review Board (IRB) approvals, if applicable? [\[N/A\]](#)
 - (c) Did you include the estimated hourly wage paid to participants and the total amount spent on participant compensation? [\[N/A\]](#)

A Proofs for Theoretical Analysis in Section 5

We heuristically explain in the main article that the proposed method is inspired by an error bound on the target domain. Here, we provide details in its derivation. To make this section self-dependent, we repeat some definitions, and further comment on their implied properties.

Definition 1 (Probabilistic Discrepancy). For two hypotheses $h, h' : \mathbb{R}^P \rightarrow \mathbb{R}$, their difference based on a probabilistic distribution D over \mathcal{X} is defined as $\gamma(h, h'|D) = \mathbb{E}_{x \sim D} |h(x) - h'(x)|$.

Definition 1 is used to quantify the distance between any two hypotheses based on a distribution D . This discrepancy is symmetric as $\gamma(h, h'|D) = \gamma(h', h|D)$. If we replace h by the ground truth outcome function, it represents the error of h' .

Definition 2 (Lipschitz Continuity). A function $f : \mathbb{R}^P \rightarrow \mathbb{R}$ is Lipschitz continuous with parameter λ , if $|f(x_1) - f(x_2)| \leq \lambda \|x_1 - x_2\|_2$ holds for any vectors $x_1, x_2 \in \mathcal{X}$. We denote the family as \mathcal{F}_λ .

In this family, for any λ , $f \in \mathcal{F}_\lambda \implies -f \in \mathcal{F}_\lambda$. We assume that the proposed hypothesis functions $\{h_0, h_1\} \in \mathcal{F}_\lambda$ which can be represented by neural networks, and the true functions $\{g_{s,0}, g_{s,1}\}_{s=1}^S \in \mathcal{F}_{\lambda^*}$.

The family of Lipschitz functions with parameter λ can also measure the Wasserstein distance between spaces. Its relationship to the Wasserstein-1 distance is described below.

$$\sup_{f: \mathcal{X} \rightarrow \mathbb{R}, \|f\|_L < \lambda} \mathbb{E}_{x \sim D} [f(x)] - \mathbb{E}_{x \sim D'} [f(x)] = \lambda W_1(D, D') \quad (10)$$

Lemma S1 (Additivity of Lipschitz functions). If $f_1 \in \mathcal{F}_{\lambda_1}$ and $f_2 \in \mathcal{F}_{\lambda_2}$, then $f_1 + f_2 \in \mathcal{F}_{\lambda_1 + \lambda_2}$.

This can be shown trivially with the triangle inequality. By the symmetry of the Lipschitz family, $f_1 - f_2, -f_1 + f_2, -f_1 - f_2 \in \mathcal{F}_{\lambda_1 + \lambda_2}$.

Lemma S2 (Symmetry of the Wasserstein distance). For any two probabilistic distributions D and D' over \mathcal{X} , $W_1(D, D') = W_1(D', D)$.

Proof. Assume that $f' \in \mathcal{F}_1$ is the function that maximizes $\mathbb{E}_{x \sim D} [f(x)] - \mathbb{E}_{x \sim D'} [f(x)]$. We have $\mathbb{E}_{x \sim D} [f'(x)] - \mathbb{E}_{x \sim D'} [f'(x)] = W_1(D, D')$. Since $f \in \mathcal{F}_1 \implies -f' \in \mathcal{F}_1$,

$$W_1(D, D') = \mathbb{E}_{x \sim D'} [-f'(x)] - \mathbb{E}_{x \sim D} [-f'(x)] \leq W_1(D', D).$$

From the other direction, we can similarly show that $W_1(D', D) \geq W_1(D, D')$, which leads to $W_1(D', D) = W_1(D, D')$. □

To bound the error on the target domain, we take a two-step procedure. First, we bound the error of the unobserved potential outcomes within each domain given the observed data. Then we explore the cross-domain relationships to bound the overall error on the target domain with labeled data from source domains.

Between-treatment Bound

For any source domain s with D_s , we want to minimize the distance between our proposed hypotheses h_0, h_1 and $g_{s,0}, g_{s,1}$. Since we are only able to observe $T = 0$ and $T = 1$ in $D_{s,0}$ and $D_{s,1}$, respectively. The full potential outcome error on D_s cannot be directly calculated. Instead, Proposition S1 suggests that this error can be bounded.

Proposition S1. For any source domain s with the marginal probabilities of receiving treatment and control as $p_s^{T=1}$ and $p_s^{T=0}$, the probabilistic discrepancy between $\{h_0, h_1\}$ and $\{g_{s,0}, g_{s,1}\}$, $\gamma(h_0, g_{s,0}|D_s) + \gamma(h_1, g_{s,1}|D_s)$ has an upper bound,

$$\gamma(h_0, g_{s,0}|D_s) + \gamma(h_1, g_{s,1}|D_s) \leq \gamma(h_0, g_{s,0}|D_{s,0}) + \gamma(h_1, g_{s,1}|D_{s,1}) + (\lambda + \lambda^*) W_1(D_{s,0}, D_{s,1}).$$

Proof. For ease of derivation, we only expand on the error bound of the control group $T = 0$, $\gamma(h_0, g_{s,0}|D_s)$. In T-learner, h_0 and h_1 are constructed separately, and they do not influence each other. The bound on $T = 1$ can be derived with identical steps.

$$\begin{aligned}
\gamma(h_0, g_{s,0}|D_s) &= \mathbb{E}_{x \sim D_s} |h_0(x) - g_{s,0}(x)| \\
&= p_s^{T=0} \mathbb{E}_{x \sim D_{s,0}} |h_0(x) - g_{s,0}(x)| + p_s^{T=1} \mathbb{E}_{x \sim D_{s,1}} |h_0(x) - g_{s,0}(x)| \\
&= p_s^{T=0} \mathbb{E}_{x \sim D_{s,0}} |h_0(x) - g_{s,0}(x)| + p_s^{T=1} \mathbb{E}_{x \sim D_{s,0}} |h_0(x) - g_{s,0}(x)| \\
&\quad - p_s^{T=1} \mathbb{E}_{x \sim D_{s,0}} |h_0(x) - g_{s,0}(x)| + p_s^{T=1} \mathbb{E}_{x \sim D_{s,1}} |h_0(x) - g_{s,0}(x)| \\
&= \gamma(h_0, g_{s,0}|D_{s,0}) + p_s^{T=1} \left(\mathbb{E}_{x \sim D_{s,1}} |h_0(x) - g_{s,0}(x)| - \mathbb{E}_{x \sim D_{s,0}} |h_0(x) - g_{s,0}(x)| \right) \\
&\leq \gamma(h_0, g_{s,0}|D_{s,0}) + p_s^{T=1} \left(\sup_{f: \mathcal{X} \rightarrow \mathcal{R}, \|f\|_L < \lambda + \lambda^*} \mathbb{E}_{x \sim D_{s,1}} [f(x)] - \mathbb{E}_{x \sim D_{s,0}} [f(x)] \right) \\
&= \gamma(h_0, g_{s,0}|D_{s,0}) + p_s^{T=1} (\lambda + \lambda^*) W_1(D_{s,0}, D_{s,1})
\end{aligned}$$

In the fifth line, we use the additivity of the Lipschitz family, $h_0 - g_{s,0} \in \mathcal{F}_{\lambda + \lambda^*}$. Similarly, between h_1 and $g_{s,1}$, we have

$$\gamma(h_1, g_{s,1}|D_i) \leq \gamma(h_1, g_{s,1}|D_{s,1}) + p_s^{T=0} (\lambda + \lambda^*) W_1(D_{s,1}, D_{s,0}).$$

With the symmetry of $W(\cdot, \cdot)$, $(\lambda + \lambda^*) W_1(D_{s,1}, D_{s,0}) = (\lambda + \lambda^*) W_1(D_{s,0}, D_{s,1})$. Then we sum up the two groups, and the bound is proven. \square

Cross-Domain Bound

In this step, we simplify the problem to a multiple domain setups but assuming randomization within each domain, $D_{s,0} = D_{s,1} = D_s$. We keep the other conditions unchanged such as the domain shift and the shift in outcome functions. As the outcomes on the target domain are unobservable, the error can still only be bounded rather than calculated. Proposition S2 suggests a bound.

Before we state the bound, we define two quantities. We assume that $w = \{w_s\}_{s=1}^{S-1}$ are weights on labeled source domains and they sum up to 1. γ_0^* and γ_1^* define the minimum discrepancies attainable for the weighted summation of all domains.

$$\begin{aligned}
\gamma_0^* &= \min_{h_0} \left[\gamma(h_0, g_{s,0}|D_s) + \sum_{s=1}^{S-1} w_s \gamma(h_0, g_{s,0}|D_s) \right]; \\
\gamma_1^* &= \min_{h_1} \left[\gamma(h_1, g_{s,1}|D_s) + \sum_{s=1}^{S-1} w_s \gamma(h_1, g_{s,1}|D_s) \right].
\end{aligned} \tag{11}$$

In (11), the two quantities depict the fundamental difference in true outcome functions across all domains, which is unoptimizable. The larger its value, the harder the target domain error can be controlled. If $g_{s,0}, g_{s,1}$ only differ slightly across domains, we are more likely to find some universally defined h_0^* and $h_1^* \in \mathcal{F}_{\lambda^*}$ that make γ_0^* and γ_1^* small.

Proposition S2. Assume that we have full randomization within each domain, and h_0^* and $h_1^* \in \mathcal{F}_{\lambda^*}$ with minimum errors γ_0^* and γ_1^* in (11). For any positive weights on source domains $w = \{w_s\}_{s=1}^{S-1}$ with $\sum_{s=1}^{S-1} w_s = 1$. The target domain error can be bounded by,

$$\begin{aligned}
\gamma(h_0, g_{s,0}|D_s) + \gamma(h_1, g_{s,1}|D_s) &\leq 2(\lambda + \lambda^*) W_1(D_s, \sum_{s=1}^{S-1} w_s D_s) + \gamma_0^* + \gamma_1^* \\
&\quad + \sum_{s=1}^{S-1} w_s [\gamma(h_0, g_{0,s}|D_s) + \gamma(h_1, g_{1,s}|D_s)].
\end{aligned} \tag{12}$$

Proof. Again, we prove it on the control group and extend it to both groups with the property of “T-learner”.

$$\begin{aligned}
\gamma(h_0, g_{S,0}|D_S) &\leq \gamma(h_0, h_0^*|D_S) + \gamma(g_{S,0}, h_0^*|D_S) \quad (\text{Triangle Inequality}) \\
&= \gamma(h_0, h_0^*|D_S) + \gamma(g_{S,0}, h_0^*|D_S) + \sum_{s=1}^{S-1} w_s \gamma(h_0, h_0^*|D_s) - \sum_{s=1}^{S-1} w_s \gamma(h_0, h_0^*|D_s) \\
&\leq \gamma(h_0, h_0^*|D_S) + [\gamma(g_{S,0}, h_0^*|D_S) + \sum_{s=1}^{S-1} w_s \gamma(g_{s,0}, h_0^*|D_s)] \\
&\quad + \sum_{s=1}^{S-1} w_s \gamma(h_0, g_{s,0}|D_s) - \sum_{s=1}^{S-1} w_s \gamma(h_0, h_0^*|D_s) \\
&= \gamma(h_0, h_0^*|D_S) - \sum_{s=1}^{S-1} w_s \gamma(h_0, h_0^*|D_s) + \gamma_0^* + \sum_{s=1}^{S-1} w_s \gamma(h_0, g_{0,s}|D_s) \\
&\leq (\lambda + \lambda^*)W_1(D_S, \sum_{s=1}^{S-1} w_s D_s) + \gamma_0^* + \sum_{s=1}^{S-1} w_s \gamma(h_0, g_{0,s}|D_s) \quad (\text{as } h_0 - h_0^* \in \mathcal{F}_{\lambda+\lambda^*})
\end{aligned}$$

Likewise, we can obtain the following quantity for the treatment group.

$$\gamma(h_1, g_{S,1}|D_S) \leq (\lambda + \lambda^*)W_1(D_S, \sum_{s=1}^{S-1} w_s D_s) + \gamma_1^* + \sum_{s=1}^{S-1} w_s \gamma(h_1, g_{1,s}|D_s)$$

Lastly, we sum over two groups to get the bound in (12). \square

Overall Bound

Proposition S1 or Proposition S2 only partially address our big goal. However, their combination gives us the overall bound on the target domain in a multicenter observational study setup.

Theorem 2 For any positive weights on source domain $w = \{w_s\}_{s=1}^{S-1}$ with $\sum_{s=1}^{S-1} w_s = 1$. The overall target domain error for the proposed hypothesis functions $\{h_0, h_1\}$ can be bounded by,

$$\begin{aligned}
\gamma(h_0, g_{S,0}|D_S) + \gamma(h_1, g_{S,1}|D_S) &\leq (\lambda + \lambda^*)[2W_1(D_S, \sum_{s=1}^{S-1} w_s D_s) + \sum_{s=1}^{S-1} w_s W_1(D_{s,0}, D_{s,1})] \\
&\quad + \sum_{s=1}^{S-1} w_s [\gamma(h_0, g_{s,0}|D_{s,0}) + \gamma(h_1, g_{s,1}|D_{s,1})] + \gamma_0^* + \gamma_1^*.
\end{aligned}$$

Proof. We replace each $\gamma(h_0, g_{0,s}|D_s)$ and $\gamma(h_1, g_{1,s}|D_s)$ in Proposition S2 with the bound derived in Proposition S1, and the overall bound can be obtained. \square

B Method Implementations and Data Preprocessing

B.1 Model Specifications

For MLP, CFR, MDMN, MDNMCFR and MDCN, we use the same model architecture for a fair comparison. The feature embedding network is parametrized through a neural network with two hidden layers of 50 units each. The outcome networks for both treatment and control groups are based on a neural network with two hidden layers of 50 units. For the circular data example and the mice data example, we set the dimensions of the embedded space to 10 and 20, respectively. The Lipschitz constraints for the Wasserstein-1 distance is maintained through the gradient penalty [19]. The tuning parameters have fixed values, as $\alpha=1e-3$ and $\beta=5e-4$. In practice, these specifications could also be tuned. We use ELU as the activation function [11] and ADAM as the optimizer [25] with step size $1e-4$ throughout both experiments. The full algorithm of MDCN is sketched out in Algorithm 1. The code will be public on Github with the MIT license when the manuscript is accepted.

Algorithm 1 MDCN Algorithm

Input: Data with treatment labels and observed outcomes, $\{\{t_i, x_i, y_i\}_{i=1}^{N_s}\}_{s=1}^{S-1}$ from source domains and unlabeled data from the target domain $\{x_i\}_{i=1}^{N_S}$.

Output: Feature embedding function ϕ , potential outcome models $\{h_0, h_1\}$, domain discriminator f_{cd} and treatment discriminator f_{bt} .

for iter = 1 to n^{iter} **do**

Sample a mini-batch from source domains $\{\{t_i, x_i, y_i\}_{i=1}^{N_s}\}_{s=1}^{S-1}$ and target domain $\{x_i\}_{i=1}^{N_S}$.

Calculate $\{l_s\}_{s=1}^S$ and update $\{w_s\}_{s=1}^S$ in (6) for cross-domain adjustment.

for iter = 1 to n_1 **do**

Sample a mini-batch from source domains $\{\{t_i, x_i, y_i\}_{i=1}^{N_s}\}_{s=1}^{S-1}$ and target domain $\{x_i\}_{i=1}^{N_S}$.

Optimize full loss in (1) with respect to the parameters in ϕ, h_0, h_1 .

Update the parameters in ϕ, h_0, h_1 .

end for

for iter = 1 to n_2 **do**

Sample a mini-batch from source domains $\{\{t_i, x_i, y_i\}_{i=1}^{N_s}\}_{s=1}^{S-1}$ and target domain $\{x_i\}_{i=1}^{N_S}$.

Optimize the cross-domain $-L_{cd}(\phi, f_{cd})$ in (7) with respect to the parameters in f_{cd} .

Update the parameters in f_{cd} .

Optimize the between-treatment $-L_{bt}(\phi, f_{bt})$ in (4) with respect to the parameters in f_{bt} .

Update the parameters in f_{bt} .

end for

end for

The method CF is implemented through the R package grf with GPL-3 license [50]. We let the model automatically tune its hyper-parameters by specifying `tune.parameters="all"`.

All Python- based methods are run on a single NVIDIA P100 GPU; the R-based CF is run on an Intel(R) Xeon(R) Gold 6154 CPU.

B.2 Preprocessing the mice data

The raw data have high variability, as the first 100 principle components only explains 50% of the total variance. Additionally, the limited sample size poses a challenge with regards to the variability assessment. To enlarge the sample size and decrease the variability of the data. We use a recently published auto-encoder for data interpolation [35]. The encoder $f_e : \mathbb{R}^{9856} \rightarrow \mathbb{R}^{15}$ is a neural network that has three hidden layers of 100 units each. The decoder $f_d : \mathbb{R}^{15} \rightarrow \mathbb{R}^{9856}$ is a neural network with one hidden layer of 50 units. Then, we construct a discriminative network: $f_i : \mathbb{R}^{15} \rightarrow [0, 1]$ with a single hidden layer of 50 units to judge the quality of interpolated data. Lastly, we add a network with no hidden layer to predict mice identity $f_m : \mathbb{R}^{15} \rightarrow [0, 1]$ ²¹.

For each domain s , we have the following loss for the control group (home cage),

$$L_{s,0} = \mathbb{E}_{x_1, x_2 \sim D_{s,0}, \alpha \sim U(0,1)} \min_{f_e, f_d, f_m} \max_{f_i} \left\{ \begin{aligned} & \left[(f_d(f_e(x_1)) - x_1)^2 + (f_d(f_e(x_2)) - x_2)^2 \right] + \end{aligned} \right. \quad (\text{I})$$

$$.1 \left[f_e(f_d(\alpha f_e(x_1) + (1 - \alpha)f_e(x_2))) - (\alpha f_e(x_1) + (1 - \alpha)f_e(x_2)) \right]^2 + \quad (\text{II})$$

$$.05 \left[CE(f_m(f_e(x_1)), s) + CE(f_m(f_e(x_2)), s) + CE(f_m(\alpha f_e(x_1) + (1 - \alpha)f_e(x_2)), s) \right] + \quad (\text{III})$$

$$.05 \left[\log(f_i(f_e(x_1))) + \log(f_i(f_e(x_2))) + \log(1 - f_i(\alpha f_e(x_1) + (1 - \alpha)f_e(x_2))) \right] \}. \quad (\text{IV})$$

We have the data reconstruction in (I). (II) is the ‘‘cycle loss’’ [35], which is to reconstruct the interpolated feature embedding. It also contributes to make f_e and f_d as reciprocal of each other. (III) is the cross-entropy loss for each domain to be predictive of its domain identity s . It is helpful in maintaining domain-specific information and creating domain shift. (IV) is the adversarial loss. It discriminates how similar interpolated points are to the raw data. Enforcing it enables the interpolation

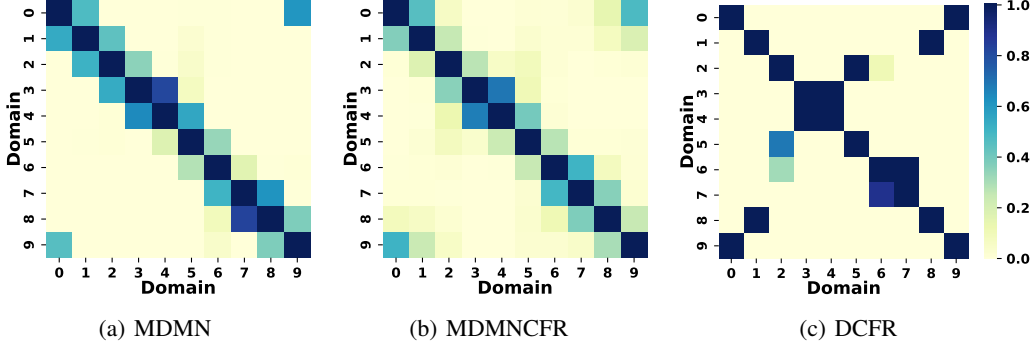


Figure S1: Additional visualizations of domain-level similarities. DCFR in 1(c) better maintains the relative closeness across domains than CFR does in Figure 2. However, it is still not appropriately capturing the original domain-level similarity as shown in 1(a) and 1(b), both of which are backed by the cross-domain adjustment.

to retain the original data distributions. The full loss is calculated by summing over all domains and all treatment groups, $\sum_{s=1}^{21} [L_{s,0} + L_{s,1}]$. We train this framework for 12,000 iterations. In each iteration, we randomly draw 20 samples from each treatment group and each domain, which makes a total batch size of 840. After the training is finished, we observe that the embedded space explains $>30\%$ of the total variance. we randomly interpolate 10,000 samples for each domain and each treatment group to make an enlarged dataset. These interpolated points overall reaches $>90\%$ accuracy in predicting the mouse identity, with $>60\%$ confidence indicated by the discriminative network f_i that they are from the true data.

For outcome models, we prepare 30 mini neural networks with input and output size: $\mathbb{R}^{15} \rightarrow \mathbb{R}$, $\{f_1^0, \dots, f_{15}^0\}, \{f_1^1, \dots, f_{15}^1\}$. These neural networks all have a single hidden layer with 15 units, and hyperbolic tangent activation functions. Their weights are initialized through the Xavier initialization [17]. Then we use 15 evenly spaced points from $[-1.5, 1.5]$ to shift their weight parameters to make them distinct. Explicitly, we shift the weight parameters in $f_s^0 \in \{f_1^0, \dots, f_{15}^0\}$ by $+(3s/15 - 1.5)$. For $\{f_1^1, \dots, f_{15}^1\}$, we shift them by another permutation of these 15 points. Lastly, they are combined with the the center of each domain s , $\bar{x}^s = \{\bar{x}_1^s, \dots, \bar{x}_{15}^s\}$ to create the overall shift in outcome functions. It encourages domains that are close in center to have similar outcome functions,

$$Y(0)|X, s \sim \mathcal{N}(\sum_{j=1}^{15} \text{sigmoid}(\bar{x}_1^s) f_j^0(X), 1); \quad Y(1)|X, s \sim \mathcal{N}(\sum_{j=1}^{15} \text{sigmoid}(\bar{x}_1^s) f_j^1(X), 1).$$

C Additional Visualizations

Figure S1 visualizes the similarity at domain level for the other 3 methods. For methods without the domain level adjustment (CFR included), we use a surrogate to calculate \mathbf{l}_s in (6), so that similarity could be represented in a comparable manner. We first use 1-d t-SNE on the learned feature embedding $\phi(x)$, as $\text{tsne}(\phi(x))$. Then we calculate the distance and weight according to (13),

$$\begin{aligned} \mathbf{l}_s &= \{l_{s,i}\}_{i \neq s}, \quad l_{s,i} = \mathbb{E}_{x \sim D_s} [\text{tsne}(\phi(x))] - \mathbb{E}_{x \sim D_i} [\text{tsne}(\phi(x))], \\ \mathbf{w}_s &= \{w_{s,i}\}_{i \neq s} = \text{softmax}(-\mathbf{l}_s). \end{aligned} \quad (13)$$

Diagonal elements are set to 1 as reference values. DCFR visualized in Figure S1 better maintains the original domain-level connectivity than CFR in Figure 3. It connect such as domains 3 and 4 or domains 6 and 7. MDMN and MDMNCFR both have the cross-domain component to learn domain similarities. They also clearly reflect the original data distributions by showing strong connectivity to two neighboring domains.

Figure S2 includes two additional t-SNE plots of the learned feature $\phi(x)$ in mouse data. In 2(a), the target domain is distant to the neighboring domains "0" and "2", which gives the model fewer relevant points to learn from to predict on the target domain. In 2(b), the treatment group and control

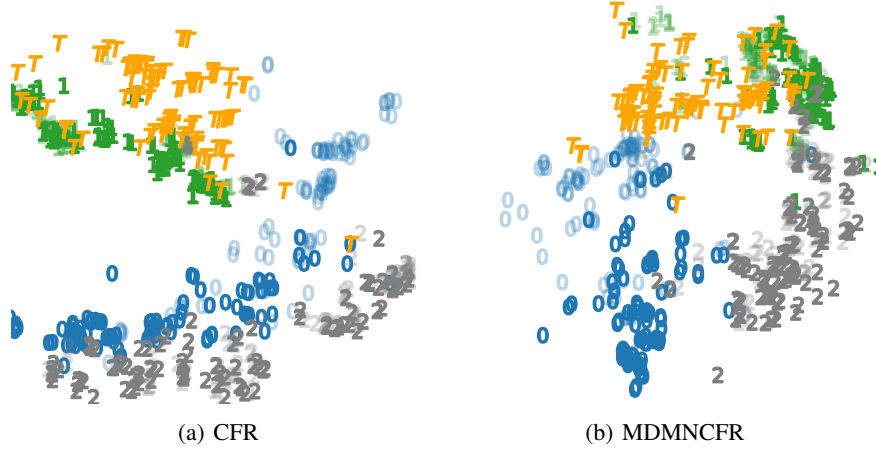


Figure S2: Additional t-SNE plots for learned $\phi(x)$. The domain 9 is chosen as the target domain and is labeled as "T". For convenience, its 3 nearest neighboring domains are labeled as "0", "1" and "2". They are found through the weight matrix in MDMN. Labels with solid shade and transparent shade represent the control group and the treatment group, respectively.

group are still less balanced compared to that in Figure 4(c), this suggests worse generalization from our bound in Theorem 1.